Supporting Information for "Antarctic Ice Sheet freshwater discharge drives substantial Southern Ocean changes over the 21st century"

Tessa Gorte[1,2], Nicole Lovenduski[1,2], Cara Nisssen [1,2], Jan Lenaerts[1], Leo

van Kampenhout[3]

[1]University of Colorado Boulder

[2]Institute of Arctic and Alpine Research

[3]Utrecht University

Contents of this file

1. Freshwater forcing

2. Expanded results

————

June 19, 2023, 8:07pm

0.1. Freshwater forcing

We define six drainage basins for the AIS: (1) the Weddell Sea, (2) the Indian Ocean, (3) the Pacific Ocean, (4) the Ross Sea, (5) the AB Seas, and (6) the Antarctic Peninsula, each of which produce different FW fluxes. The historical fluxes are taken from ? (?) which separates calving fluxes (solid ice) from basal melt fluxes (liquid water). Historically, calving and basal melt represent 48% and 52% of the total AIS FW flux, respectively, but this varies greatly from basin to basin. The FW forcing from the Antarctic Peninsula, for instance, is 13% calving and 87% basal melt compared to 74% calving and 26% basal melt for the Weddell Sea. Due to the sparse observations of AIS FW fluxes, we assume the calving to basal melt ratio persists into the future for every basin. The only drainage basin for which we adjust the FW discharge is the AB Seas basin which increases from 1992-2020 per a linear fit of the data published by ? (?). From 2021 through the end of the simulation period, we follow results from ? (?). By the end of the century, the AB Seas' flux increases from 716 Gt y^{-1} to 7039 Gt y^{-1} (still at a ratio of 32% calving to 68% basal melt).

0.2. Expanded results

For the first 15 years of the shared simulation period (1992-2007; beginning of simulation (BoS)) the upper ocean (top 200 m) stratification varies between 0-1 kg m^{-3} for both simulations. By the final 15 years (2085-2100, end of simulation (EoS)), the added FW engenders a ∼3 kg m^{-3} stronger stratification in the AB Seas region in the IMBIE simulation. Taking the difference in each simulation over time (Figure S2, panels C and F), we find that there is little difference in the CONTROL simulation while an increased stratification signal (> 1 kg m^{-3}) manifests most strongly in the AB Seas and permeates

into the Weddell and Ross Seas. With little change in the CONTROL simulation, the difference in the temporal evolution (Figure S2, panel I), then, shows a similar signal to that of the IMBIE simulation.

From the surface to (and below) 500 m, the SO warms ubiquitously. Close to the AIS, the surface SO is ∼0 °C at the BoS and increases to ∼2 °C by the EoS (Figure S3, panels A-F). Compared to the CONTROL, the IMBIE simulation produces a ∼ 0.3°C cooler surface ocean. Regions of anomalously cooler waters develop in the AB Seas region and off the coast of the Eastern AIS, near the historical sea ice edge (Figure S3, panel I). Like the surface, the temperature at 100 m depth (T_{100}) is also ∼0 °C at the BoS in both simulations and both warm over the 21st century (Figure S4, panels A-F). Toward the EoS, the IMBIE simulation is anomalously warmer particularly close to the coast in the AB Seas region. This warming signal also manifests strongly (> 1 °C) in the Ross Sea and to a lesser extent (> 0.5 °C), in the Weddell Sea as well (Figure S4, panel I). The differences in temporal evolution of temperature at 200 m depth ($T_2$00) between the two simulations becomes more spatially variable with anomalous cooling north of 60 °S and significant anomalous warming south of 60 °S (Figure S5, panels A-F). The strongest warming signals (> 1 °C) are close to the coast in the AB, Weddell, and Ross Seas as well as the Antarctic Peninsula. Offshore, there is further warming in excess of 0.25 °C all around the AIS including the Indian and Pacific Ocean drainage basins (Figure S5, panel I). 500 m below the surface is approximately the depth at which the entire zonally-averaged SO is warmer in the IMBIE than the CONTROL (Figure 4). At this depth, the historical temperatures (T_{500}) increase by 0.25-2 °C over the course of the century in both simulations. On the continental shelf and beyond, the IMBIE simulation traps

significantly more heat than the CONTROL. This signal is particularly robust in the coastal western Ross Sea with differences exceeding 1 °C between the two simulations. As with T_{200}, offshore heat is trapped all around the AIS, extending out to nearly 45 °S in the southern Pacific and southern Atlantic Oceans.
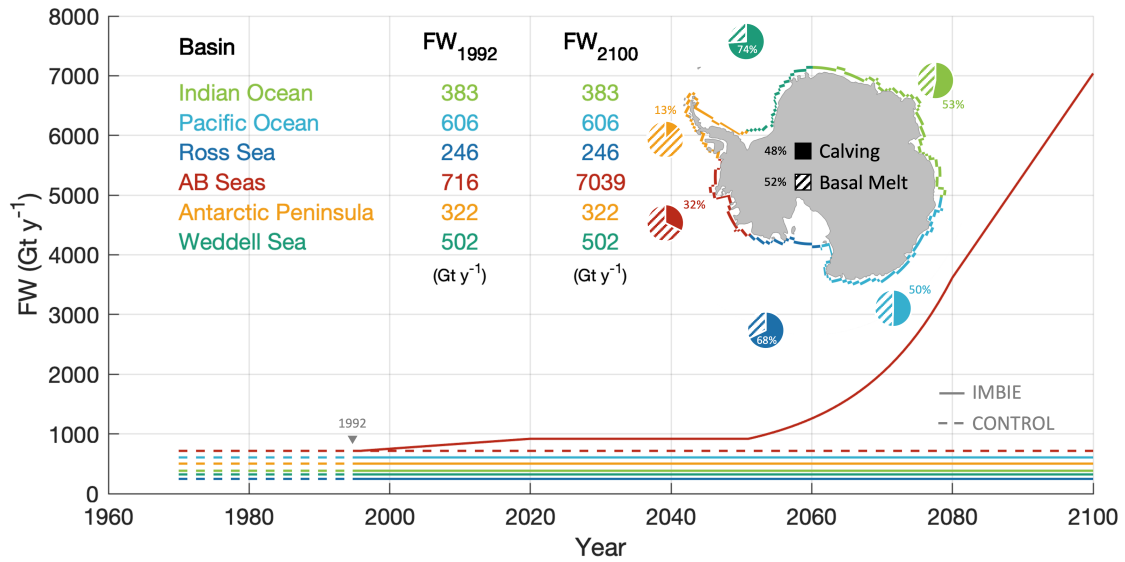
Figure S1. The AIS FW distribution shown spatially and as a time series. The 6 basins we define are the Weddell Sea (dark green), the Indian Ocean (light green), the Pacific Ocean (light blue), the Ross Sea (dark blue), the AB Seas (red), and the Antarctic Peninsula (orange). Each basin has its own ratio of calving to basal melt as depicted by the pie charts (percentages denote the percent of FW flux realized as calving). The time series show the total FW fluxing from each basin for the CONTROL (dashed) and the IMBIE (solid) simulations; the latter of which branches off in 1992. Also displayed are the values of total FW fluxing from each basin in 1992 and in 2100 in Gt y^{-1}.
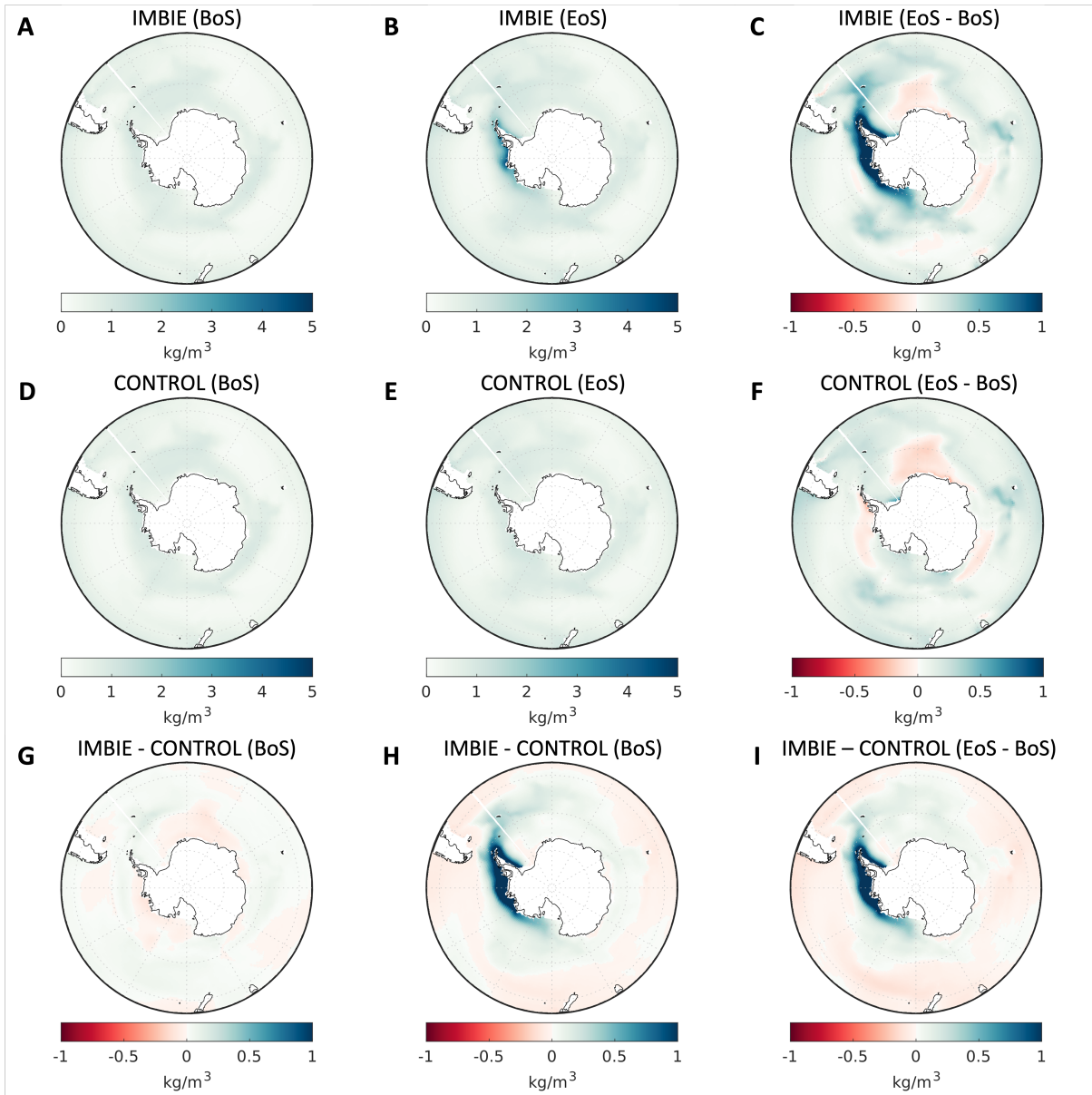
Figure S2. Snapshots of density stratification (200 m - surface) for the IMBIE simulation (top row), CONTROL simulation (middle row), and the difference (IMBIE - CONTROL; bottom row). The columns depict the average stratification for the periods of 1992-2007 (left), 2085-2100 (center), and the difference (right).
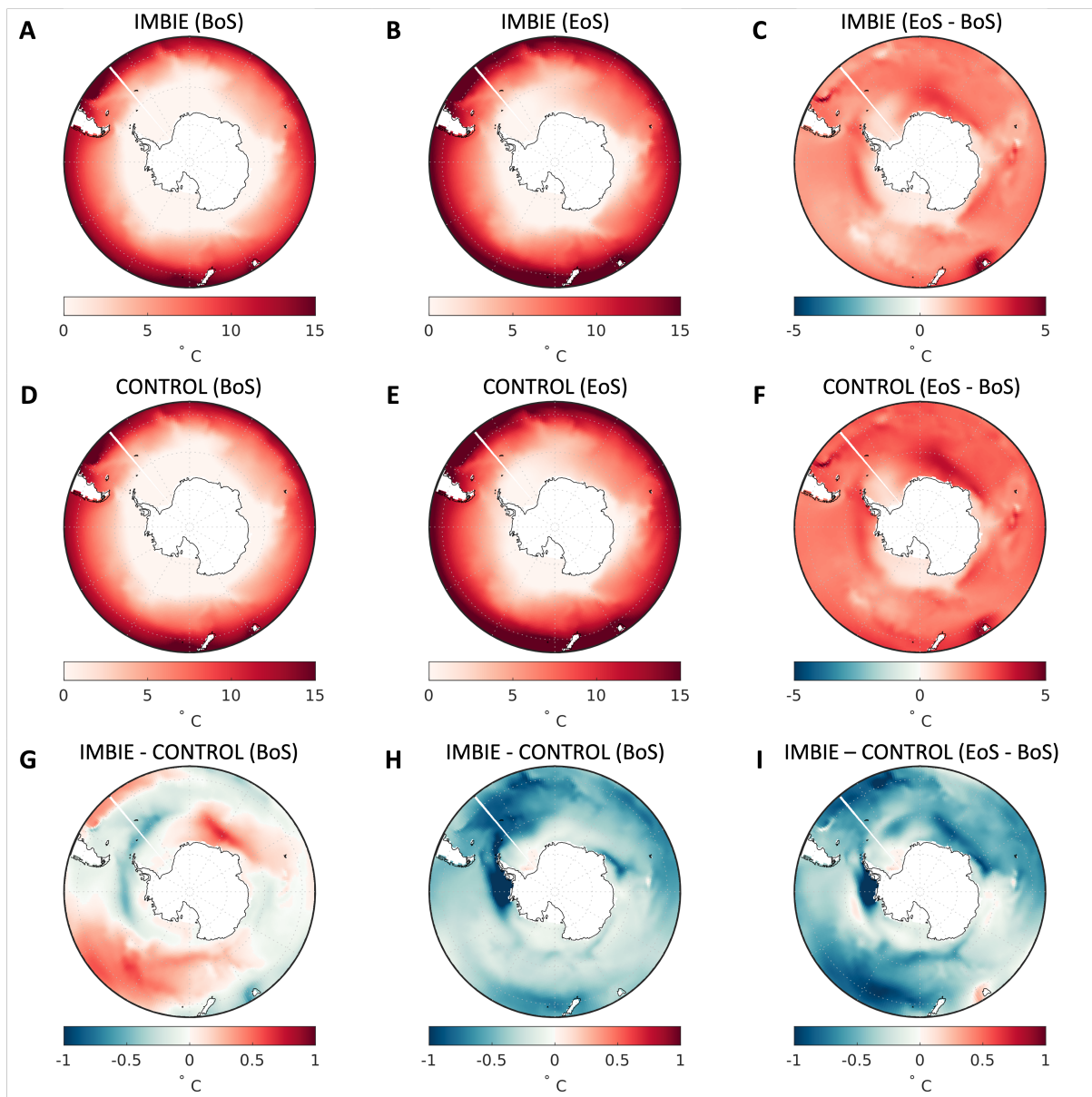
Figure S3. Snapshots of surface temperature for the IMBIE simulation (top row), CONTROL simulation (middle row), and the difference (IMBIE - CONTROL; bottom row). The columns depict the average surface temperature for the beginning of the simulation (BoS) from 1992-2007 (left), the end of the simulation (EoS) 2085-2100 (center), and the difference (right).
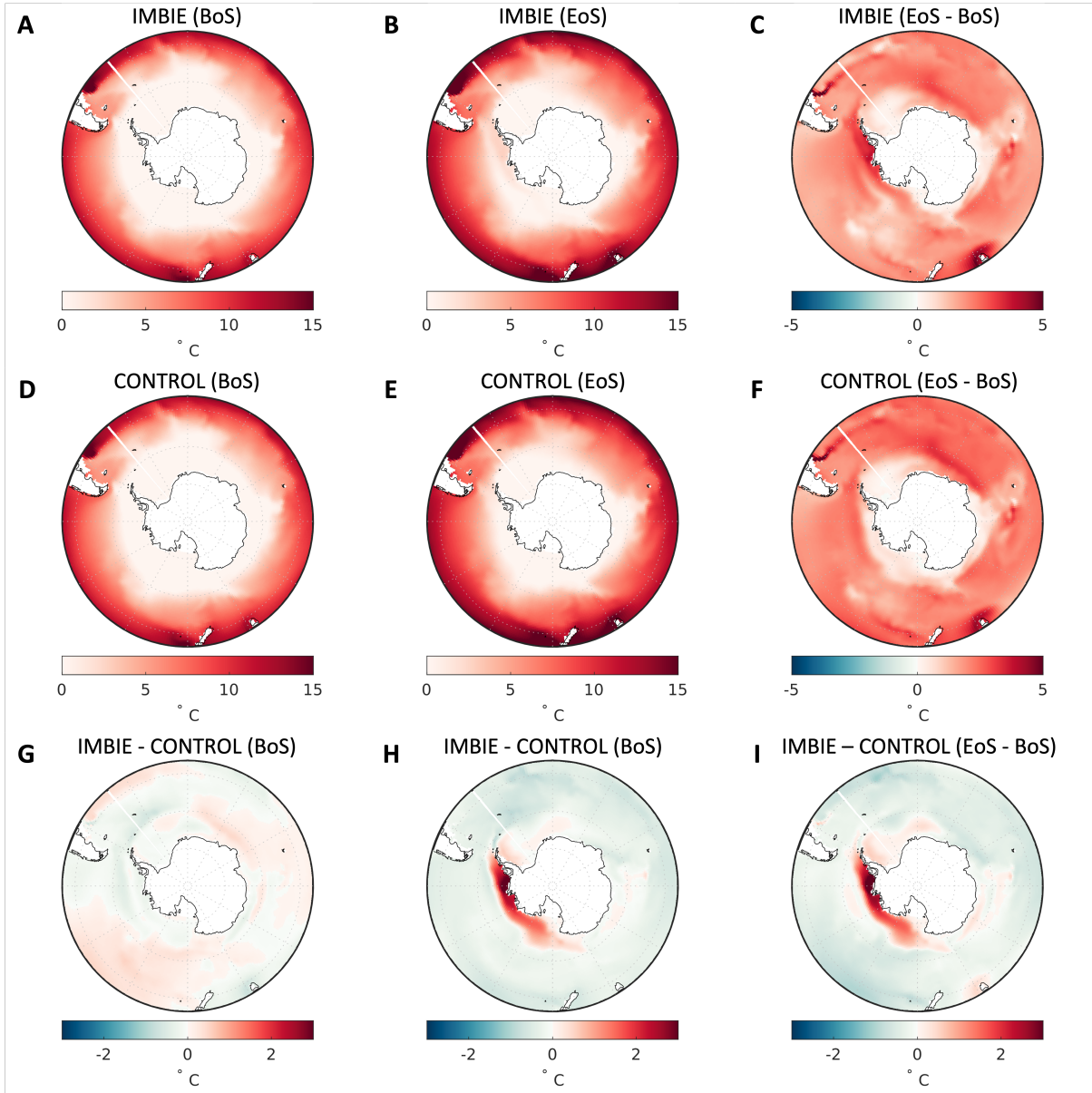
Figure S4. Snapshots of T_{100} for the IMBIE simulation (top row), CONTROL simulation (middle row), and the difference (IMBIE - CONTROL; bottom row). The columns depict the average T_{100} for the beginning of the simulation (BoS) from 1992-2007 (left), the end of the simulation (EoS) 2085-2100 (center), and the difference (right).
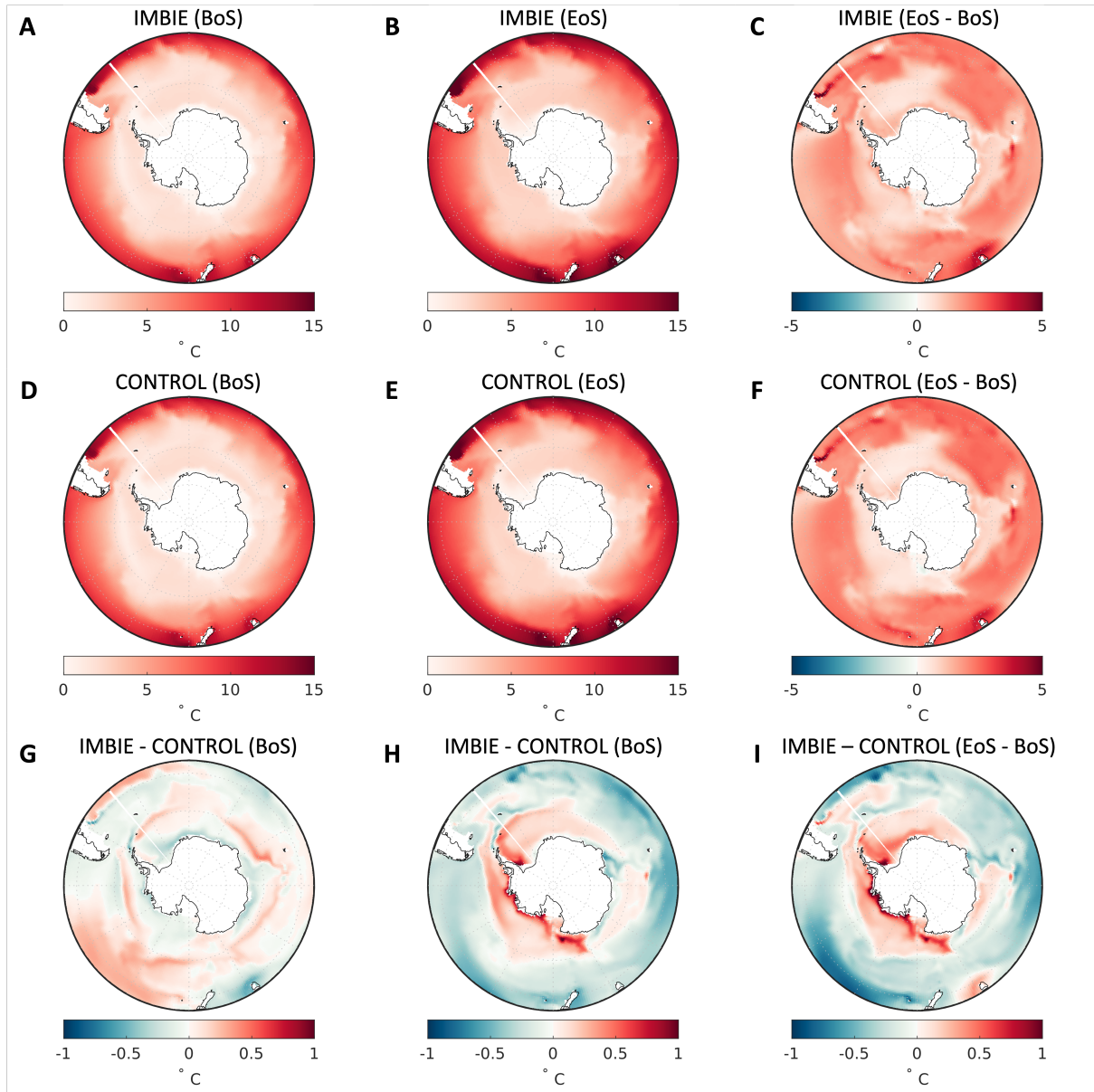
June 19, 2023, 8:07pm

Figure S5. Snapshots of T_{200} for the IMBIE simulation (top row), CONTROL simulation (middle row), and the difference (IMBIE - CONTROL; bottom row). The columns depict the average T_{200} for the beginning of the simulation (BoS) from 1992-2007 (left), the end of the simulation (EoS) 2085-2100 (center), and the difference (right).
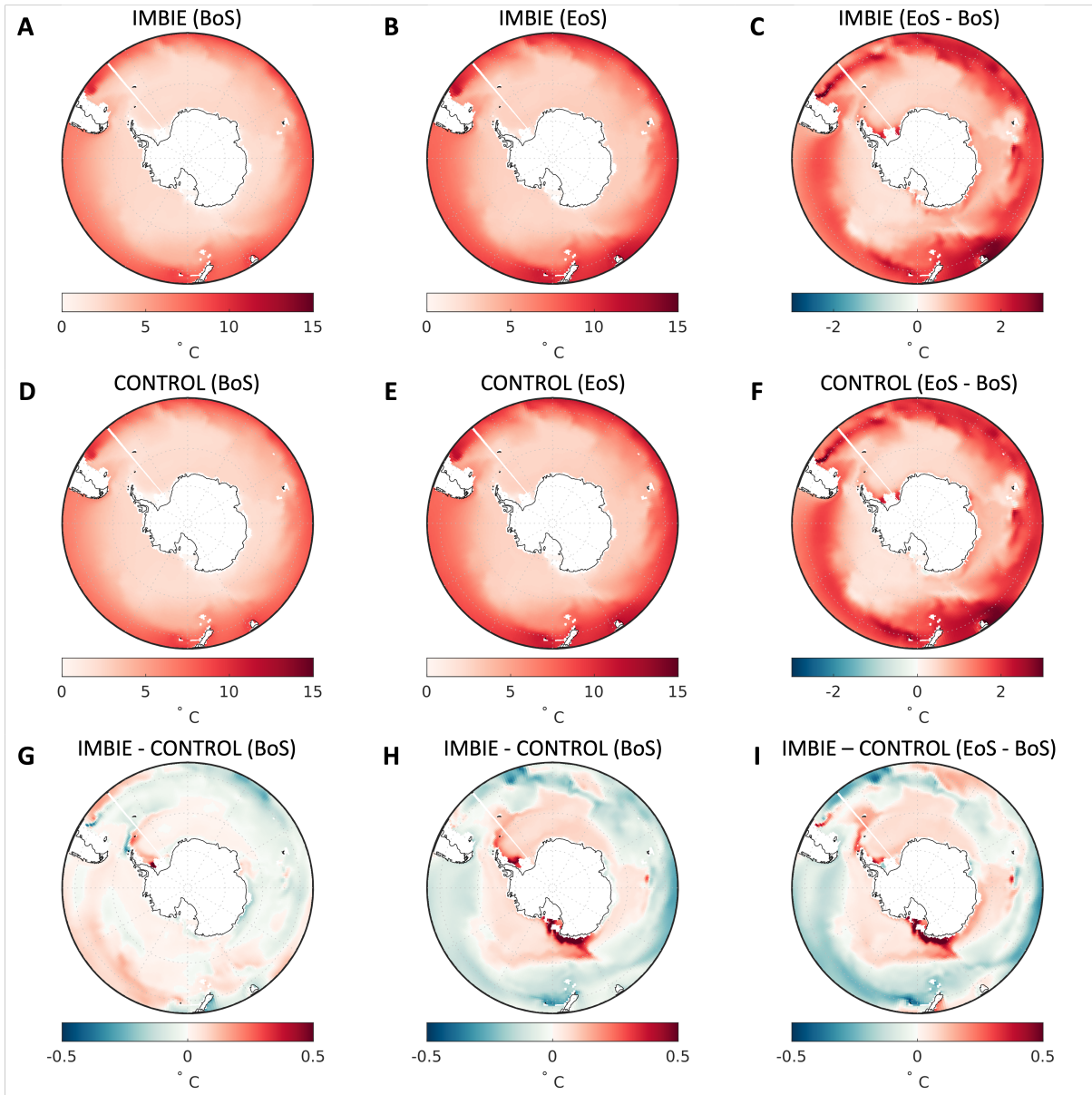
June 19, 2023, 8:07pm

Figure S6. Snapshots of T_{500} for the IMBIE simulation (top row), CONTROL simulation (middle row), and the difference (IMBIE - CONTROL; bottom row). The columns depict the average T_{500} for the beginning of the simulation (BoS) from 1992-2007 (left), the end of the simulation (EoS) 2085-2100 (center), and the difference (right).